Microchemical Journal 217 (2025) 114915

Contents lists available at ScienceDirect

Microchemical Journal

journal homepage: www.elsevier.com/locate/microc

High-performance nonenzymatic creatinine detection by Cu-MOF@MXene electrochemical sensor

Xianglong Bian [a,1], Dong Yang [b,1], Lin Chen [a], Yingfei Zeng [a], Li Zhu [a], Hua Pei [a], Qianfeng Xia [a], Paul K. Chu [c,*], Tingwei Hu [a,d,**]

[a] NHC Key Laboratory of Tropical Disease Control, School of Tropical Medicine, Hainan Medical University, Haikou 571199, Hainan, China.
[b] School of Biomedical Information and Engineering, Hainan Medical University, Haikou 571199, Hainan, China.
[c] Department of Physics, Department of Materials Science and Engineering, and Department of Biomedical Engineering, City University of Hong Kong, Tat Chee Avenue, Kowloon, Hong Kong, China.
[d] State Key Laboratory for Mechanical Behavior of Materials, Xi'an Jiaotong University, Xi'an 710049, Shaanxi, China.

ARTICLE INFO

Keywords:
Creatinine detection
Cu-MOF@MXene
Nonenzymatic electrochemical sensor

ABSTRACT

Creatinine serves as a crucial biomarker for various diseases, and the development of effective and stable nonenzymatic sensor is essential due to the limitations of enzyme-based biosensors, such as poor conductivity and environmental instability. In this study, a composite material comprising a copper organic framework and MXene (Cu-MOF@MXene) is synthesized through a one-step reaction, enabling enzyme-free electrochemical sensing of creatinine. The Cu-MOF@MXene sensor demonstrates good linearity within the range of 20.0 μM to 150.0 μM and a low detection limit (LOD) of 20.069 μM. A screen-printed electrode (SPE) coated with Cu-MOF@MXene is fabricated for monitoring urine and human serum samples. The results indicate that the SPE possesses high sensitivity, selectivity, and stability for nonenzymatic creatinine detection, highlighting potential advancement in clinical testing and medical diagnostics.

1. Introduction

Kidney diseases have emerged as a chronic and global health concern [1]. Creatinine (2-amino-1-methyl-2-imidazolin-4-one, Cre) is a waste product of muscle metabolism, primarily excreted by the kidneys [2]. The concentration of creatinine in the human body serves as a critical indicator of kidney function, reflecting the kidneys' ability to filter blood [3]. In healthy individuals, the physiological concentrations of creatinine are typically 35–140 μM in serum and 71–265 μM in urine [4]. Several methods are available for creatinine detection, including the Jaffe method, enzymatic assays, and high-performance liquid chromatography (HPLC) [5,6]. While the Jaffe reaction is a straightforward and cost-effective colorimetric method [7], it is prone to interferences from substances in the blood, such as acetone, vitamin C, and glucose [5]. These substances can react with the basic picric acid, leading to a red color and compromising the specificity of serum creatinine detection [8]. Enzymatic methods offer high specificity and sensitivity but are often expensive [9] and can be affected by endogenous creatine, bilirubin, ascorbic acid, and certain clinical medications [10]. HPLC coupled with fluorescence is an advanced technique for creatinine measurement [11], but it requires complex sample preparation, cumbersome analytical procedures, and costly reagents [12]. Therefore, there is a strong need for a rapid, stable, and economical alternative technique for creatinine detection in modern clinical diagnostics.

In recent years, electrochemical analysis methods have gained significant importance in both bioanalysis and environmental analysis. Within the realm of bioanalysis, electrochemical biosensors have experienced rapid development, primarily due to their rapid response times and high sensitivity [13]. These sensors are capable of detecting small molecules, nucleic acids, proteins, and cells with exceptional sensitivity. By employing strategies such as layered structure electrodes, nanomaterial modifications, and sophisticated mathematical algorithms for data analysis, they facilitate highly sensitive and selective direct analysis of a wide range of biological small molecules [14,15]. Furthermore,

* Corresponding author.
** Corresponding author at: NHC Key Laboratory of Tropical Disease Control, School of Tropical Medicine, Hainan Medical University, Haikou 571199, Hainan, China.
E-mail addresses: paul.chu@cityu.edu.hk (P.K. Chu), htingwei1236@mail.xjtu.edu.cn (T. Hu).
[1] Xianglong Bian and Dong Yang contributed equally to this work and should be considered as co-first authors.

https://doi.org/10.1016/j.microc.2025.114915
Received 2 May 2025; Received in revised form 12 July 2025; Accepted 13 August 2025
Available online 19 August 2025

miniaturized electrochemical sensing platforms are increasingly being researched, offering a cost-effective, disposable, and reusable rapid analysis platform for point-of-care testing in medical settings [16]. In the field of environmental analysis, electrochemical methods excel in their high sensitivity and fast analysis speed, particularly for the detection of heavy metal ions, making them a focal research area. These advancements have not only propelled the development of electrochemical analysis technology but also provided robust tools for biomarker detection, disease monitoring, and environmental surveillance [17,18].

For the detection of creatinine molecules, electrochemical methods are renowned for their speed and sensitivity [19–23]. Electrochemical biosensors are broadly categorized into two types: enzymatic and nonenzymatic. Enzymatic biosensors, while effective, have several drawbacks, including complex preparation processes, poor conductivity, and susceptibility to environmental factors [24,25]. These limitations result in high background signals, a narrow detection range, short storage life, and reduced stability [26,27]. In contrast, nonenzymatic biosensors leverage interactions between creatinine and nanomaterials to overcome the limitations of their enzymatic counterparts [28,29]. For instance, metal nanoparticles and metal-organic frameworks (MOFs) have shown great promise in this regard. [30,31]. These metal nanoparticles can be integrated into nonenzymatic biosensors for creatinine detection [32].

MOFs offer a large specific surface area, high porosity, and multiple active sites [33,34]. Characterized by their nanoporous structures and metal ions linked to organic ligands, MOFs have emerged as a promising alternative to traditional metal nanoparticles [35,36]. Different types of materials can be combined with MOFs to enhance their performance. For example, MXene, a two-dimensional (2D) material, can be coupled with MOFs to improve stability and electrical conductivity [37,38]. Wang et al. developed a molecularly imprinted electrochemical sensor modified with Cu-MOF and $Ti_3C_2T_x$ for the detection of hygromycin B in food [39]. Qi et al. prepared an electrochemical sensor based on Fe-MOF-NH_2/CNTs-NH_2/MXene for the rapid and sensitive detection of ofloxacin [40]. These composites not only preserve the intrinsic attributes of MOFs but also offer additional benefits such as electrical conductivity, magnetic responsiveness, optical functionality, and catalytic activity [41]. The 2D MXene is produced by selectively etching group IIIA-VA elements from the MAX phase, which consists of thin layers of metal carbides or nitrides [42,43]. MXene offers many advantages, including adjustable interlayer spacing, a hydrophilic surface, high metallic conductivity, and a plethora of surface functional groups [44,45]. These characteristics render MXene highly promising in electronics, sensing, catalysis, and biomedical fields [46,47].

In this study, the Cu-MOF@MXene is synthesized through a cost-effective one-step process using inexpensive reactive precursors. This material exhibits unique structural and performance advantages, making it highly suitable for nonenzymatic electrochemical sensing of creatinine. The Cu-MOF@MXene retains the high specific surface area and porous structure of MOFs while integrating the 2D layered characteristics of MXene. The three-dimensional (3D) structure of Cu-MOF enhances the material's adsorption capacity, and the MXene layers increase conductivity, improving the electrochemical performance for creatinine detection. The Cu-MOF@MXene electrode demonstrates a good linear range (20.0 μM to 150.0 μM) and a low detection limit (20.069 μM) for creatinine. The electrochemical properties of Cu-MOF@MXene surpass those of both Cu-MOF and MXene. Additionally, a screen-printed electrode (SPE) coated with Cu-MOF@MXene is successfully fabricated and applied to detect creatinine in urine and human serum samples. Benefiting from the high electrical conductivity, excellent stability, and selectivity of Cu-MOF@MXene, the SPE shows high sensitivity, high selectivity, and good reproducibility in the electrochemical detection of creatinine. These properties enable accurate detection of creatinine in complex biological samples without interference from other substances. This study not only introduces a cost-effective approach for synthesizing composite materials but also provides valuable insights and references for the advancement of high-performance biosensors in clinical and medical diagnostics.

2. Experimental details

2.1. Chemicals and materials

Titanium aluminum carbide (Ti_3AlC_2) was purchased from RHAWN Chemical Reagent Co., Ltd. (Shanghai, China). Lithium fluoride (LiF), potassium ferricyanide ($K_3Fe(CN)_6$), potassium ferrocyanide ($K_4Fe(CN)_6$), cupric chloride ($CuCl_2$), polyvinylpyrrolidone (PVP), polyphthalic acid, and 1,3,5-benzenetricarboxylic acid ($C_9H_6O_6$) were supplied by MACKLIN Chemical Reagent Co., Ltd. (Shanghai, China). Sodium chloride (NaCl), methanol, potassium chloride (KCl), disodium phosphate ($Na_2HPO_4 \cdot 12H_2O$), and sodium dihydrogen phosphate trihydrate ($NaH_2PO_4 \cdot 3H_2O$) were purchased from Xilong Chemical Co., Ltd. (Guangdong, China). Sulfuric acid (H_2SO_4) and concentrated hydrochloric acid (HCl) were bought from Cologne Chemical Reagent Co., Ltd. (Chengdu, China). All the chemicals were analytical grade and used without further treatment. Deionized water (DW) was used throughout the experiments. The phosphate buffer solution (PBS, 0.01 M, pH = 7.4) was prepared with $Na_2HPO_4{\cdot}12H_2O$, $NaH_2PO_4{\cdot}3H_2O$, KCl, and NaCl.

2.2. Synthesis

MXene was synthesized according to an established protocol [48]. Briefly, 3.2 g of LiF was homogenized with 40 mL of 9.0 M HCl at 40 °C for 15 min under continuous magnetic stirring. Subsequently, 2.0 g of Ti_3AlC_2 precursor was gradually introduced into the etchant solution and reacted for 48 h under inert nitrogen atmosphere. The resultant suspension underwent sequential purification steps: centrifugation (3500 rpm, 2 min), repeated washing cycles with 2.0 M HCl followed by DW until neutral pH was attained, and vacuum filtration through a 0.2 μm membrane. The multi-layer MXene solution was centrifuged at 3500 rpm for 30 min to produce the single-layer MXene. The MXene powder was prepared by freeze-drying. The synthesis of Cu-MOF was based on information in the literature [49]. The synthesis of Cu-MOF was initiated by dissolving 5.0 g of $Cu(NO_3)_2{\cdot}3H_2O$ in 100 mL of methanol, resulting in a transparent blue solution. In a separate step, 1.0 g of PVP and 2.91 g of $C_9H_6O_6$ were dissolved in 100 mL of methanol, and the mixture was sonicated to form a clear solution. The copper nitrate solution was then slowly added to the PVP and $C_9H_6O_6$ solution at a rate of 300 μL/min under vigorous stirring. The resulting mixture was continuously stirred for 24 h, yielding a blue suspension. Finally, the Cu-MOF powder was obtained by freeze-drying the suspension.

Solution A was prepared by dissolving an appropriate amount of $CuCl_2$ in methanol under continuous magnetic stirring to achieve a final concentration of 0.1 M. In parallel, the pH of a 0.1 M polyphthalic acid solution was systematically adjusted to 6.0 through dropwise addition of 1.0 M KOH solution while monitoring with a calibrated pH meter.The synthesis of Cu-MOF@MXene composite was initiated by dispersing a precisely measured amount of single-layer MXene in deionized water to form solution B of 0.1 M. Solution A was then introduced into solution B via a peristaltic pump at a controlled rate of 5 drops/min (approximately 0.25 mL/min) under continuous magnetic stirring. The reaction mixture was maintained at room temperature with vigorous stirring (3000 rpm) for 48 h to ensure complete coordination. The resulting composite underwent sequential purification: (1) triple washing with absolute ethanol (99.9%) to remove residual reactants and byproducts, (2) centrifugation at 3500 rpm for 15 min, (3) vacuum filtration through a 0.2 μm membrane, and (4) lyophilization at −40 °C under 0.1 mbar for 24 h. To optimize the composite structure, we systematically investigated the $CuCl_2$/MXene mass ratio by preparing four different formulations (2,1, 2,2, 2,3, 2:4). Comprehensive characterization revealed that the 2:3 ratio yielded the optimal structural integrity and functional performance. The preparation of the Cu-MOF@MXene composite was

achieved by mixing a $CuCl_2$ solution with a monolayer MXene dispersion under controlled conditions. In this process, Cu-MOF nanoparticles were uniformly anchored onto the MXene surface, forming a homogeneous coating layer. The anchoring mechanism primarily involves coordination interactions between Cu^{2+} ions and the surface functional groups (e.g., —OH and —F) of MXene, which can be represented as: MXene + Cu^{2+} → MXene-Cu^{2+}. This coordination not only strengthens the interfacial bonding between Cu-MOF and MXene but also enhances the composite's electrical conductivity and structural stability, thereby significantly improving its electrocatalytic performance for creatinine detection.

2.3. Materials characterization

The morphological characteristics and structural features of the synthesized samples were characterized by scanning electron microscopy (SEM, ZEISS Sigma 300), and the elemental composition analysis and spatial distribution mapping were performed through energy-dispersive X-ray spectroscopy (EDS) coupled with the SEM system. For crystallographic characterization, powder X-ray diffraction (PXRD) patterns were acquired using a PANalytical X'Pert PRO diffractometer equipped with a monochromatic Cu Kα radiation source (λ = 1.5406 Å). Raman spectroscopic analysis was conducted on a Renishaw inVia Qontor confocal Raman microscope system, utilizing a 633 nm He—Ne laser excitation source with a power output of 1.5 mW and a spectral resolution of 1 cm^{-1}.

2.4. Electrode preparation

The glassy carbon electrode (GCE, 3 mm in diameter) was polished with α-alumina powders (0.5 μm, 0.3 μm, and 0.05 μm), cleaned ultrasonically in ethanol and DW for several minutes, and dried in a vacuum oven. Electrochemical activation of the polished electrode was carried out in 1.0 mM H_2SO_4 solution using CV with the following parameters: potential window of −1.0 V to +1.0 V (vs. Ag/AgCl), scan rate of 100 mV/s, and 20 consecutive cycles. This activation process served to enhance the electrode's electrochemical activity while removing surface contaminants. Following activation, the electrode's electrochemical performance was evaluated in a 0.1 M KCl solution containing equimolar concentrations (1.0 mM each) of $K_3[Fe(CN)_6]$ and $K_4[Fe(CN)_6]$. The CV measurements were performed within a potential range of −0.2 V to +0.6 V (vs. Ag/AgCl) at a scan rate of 50 mV/s. Under standardized laboratory conditions, the optimized electrode exhibited a peak potential separation (ΔEp) of less than 80 mV, with values approaching the theoretical ideal of 64 mV for a reversible one-electron transfer process. If the electrode failed to meet these criteria, it was reprocessed meeting the standard. In the fabrication of Cu-MOF@MXene/GCE, 2.0 mg of Cu-MOF@MXene and 50.0 μL of Nafion solution (5.0%) were dissolved in 2.0 mL of DW and sonicated for 30 min to form a homogenous Cu-MOF@MXene suspension (0.98 g/L). Nafion is indeed an ionic polymer with inherent ion-exchange properties. In this study, the 5% Nafion solution was solely employed as a binder and dispersant to effectively immobilize the Cu-MOF@MXene composite on the working electrode surfaces and prevent its detachment during electrochemical measurements in aqueous solutions. Its primary role is mechanical stabilization rather than participation in the sensing mechanism. As shown in Fig. S4, we have experimentally verified that Nafion does not contribute to the sensor's response for creatinine detection. A Nafion-modified control electrode (without composite) was prepared and subjected to CV tests in both creatinine-free and creatinine-containing PBS solutions. As shown in Fig. S4, no identifiable redox peaks for Cu/Cu^{2+} were observed. Furthermore, even after adding creatinine at concentration, the CV curves exhibited no significant or specific changes. A 10.0 μL drop of the suspension was applied to the GCE surface and vacuum-dried to form the film on the electrodes (7.07×10^{-4} cm^2). The sensor preparation and detection processes are illustrated in Fig. 3. For comparison, MXene/GCE and Cu-MOF/GCE were prepared by a similar procedure.

2.5. Electrochemical evaluation

All electrochemical measurements were performed using a CORRTEST electrochemical workstation (Wuhan Corrtest Instruments Corp., China), with subsequent data analysis conducted through the dedicated CS Studio 6.0 software package. At room temperature, a cylindrical electrolyzer was connected to the standard three-electrode system (working electrode, reference electrode, and counter electrode). The GCE with Cu-MOF, MXene, or Cu-MOF@MXene was the working electrode, Ag/AgCl was the reference electrode, and platinum was the counter electrode. The electrochemical properties of different electrodes were investigated in 0.01 M PBS by CV in the potential range between −0.5 and +0.5 V at a scanning rate of 50 mV/s using a potential interval of 0.5 mV. Electrochemical impedance spectroscopy (EIS) was performed at room temperature. The 0.1 M KCl solution containing equimolar concentrations (5.0 mM each) of $K_3[Fe(CN)_6]$ and $K_4[Fe(CN)_6]$ was used, and the frequency range was from 0.1 to 10^5 Hz. The sensor performance is notably influenced by environmental conditions, particularly pH. At physiological pH (7.4), optimal charge balance between creatinine and the Cu-MOF@MXene surface ensures stable detection, as evidenced by the PBS-based measurements. While temperature and humidity effects require systematic study, room-temperature operation demonstrated herein yielded reproducible results. Future investigations will quantify these parametric sensitivities for point-of-care applications.

2.6. Screen-printed electrode (SPE)

The progressive advancement in electroanalytical methodologies necessitates the development of innovative sensing platforms [50]. The SPE offers distinct advantages, particularly in enabling the miniaturization of electrochemical systems while maintaining robust analytical performance. The three essential electrochemical components were integrated on a single substrate, including the working electrode, reference electrode, and counter electrode. This integration allowed the analysis of samples with a volume as small as a few milliliters or even microliters. The SPE functionality was monitored by connecting the wires of lectrochemical workstation to silver conductive layer beneath the SPE. This connection ensured that three electrodes functioned effectively and robustly for different electroanalytical applications. In the fabrication of Cu-MOF@MXene/SPE, 2.0 mg of Cu-MOF@MXene and 50.0 μL of Nafion solution were dissolved in 2.0 mL of DW and sonicated for 30 min to form the Cu-MOF@MXene suspension (0.98 g/L). The 10.0 μL of suspension was placed on the SPE and vacuum-dried to form the film on the electrode.

2.7. Real sample analysis

1.0 mL of fresh urine obtained from a healthy participant was diluted with 100 mL of 0.01 M PBS (pH = 7.4) to form the electrolyte. The dilution step was instrumental in reducing the concentrations of the electrolyte and impurities in the urine for a more controlled analysis matrix. The urine was stored at 4 °C for subsequent experiments.

The human serum samples were provided by the Second Affiliated Hospital of Hainan Medical University with informed consent. This study involves the use of patient serum samples, which has been approved by the relevant ethics committee or institution. All research procedures adhere to the ethical principles of the Declaration of Helsinki, ensuring that the use of patient serum samples meets the high ethical standards required for medical research. The total blood samples were collected randomly and the serum (100 μL) was obtained by centrifugation and stored at 4 °C.

3. Results and discussion

Fig. 1(a) depicts the preparation procedure of the Cu-MOF@MXene composite. Initially, single-layered MXene is prepared through ultrasonic HCl/LiF etching. The layered structures of MXene are characterized by SEM [Fig. S1(a) and S1(b)] and TEM [Fig. S1(c) and S1(d)]. Generally, single-layered MXene displays a nano-sheet structure, where the individual nanosheets can attain dimensions as large as 1 μm [48]. These nano-sheet structures are relatively flat, characterized by good flexibility and plasticity. MXene surface is rich in oxygen-containing functional groups, which can significantly influence its properties. The single-layered MXene undergoes freeze-drying, resulting in an interlayer structure that is open and non-compact [38]. This facilitates the diffusion of ions and molecules, thereby enhancing its potential in the realms of energy storage and catalysis. Subsequently, due to the reducing property of MXene, Cu-MOF@MXene composite is fabricated through a one-step reaction involving single-layered MXene and $CuCl_2$. The $CuCl_2$/MXene ratio plays a pivotal role in determining the electrochemical performance of composites. To elucidate this effect, SEM analysis is conducted on composites synthesized with $CuCl_2$/MXene mass ratios of 2:1, 2:2, 2:3, and 2:4. The morphological evolution with ratio variation is illustrated in Figs. 1(b)-(e). When the $CuCl_2$/MXene is 2:3, the obtained morphological structure is distinctly different from those of other ratios, confirming the formation of Cu-MOF@MXene composite.

Fig. 1(f) displays the CV curves of the four modified electrodes recorded over a potential range of −0.3 V to +0.7 V at a scanning rate of 50 mV/s, using a 0.1 M KCl solution containing 1.0 mM $K_3[Fe(CN)_6]$ and 1.0 mM $K_4[Fe(CN)_6]$ as the supporting electrolyte. In order to identify the optimal composite, four distinct modified electrodes are fabricated by the four composites. To ensure consistency, all electrochemical experiments are conducted under identical room temperature and pH conditions. The bar chart in the inset demonstrates the response intensity values for creatinine detection using CV. Among the electrodes, the Cu-MOF@MXene/GCE with a $CuCl_2$/MXene ratio of 2:1 (black curve) exhibits relatively low current density. Upon increasing the MXene content and adjusting the $CuCl_2$/MXene ratio to 2:2, a notable enhancement in current density is observed (red curve). Further increasing the $CuCl_2$/MXene ratio to 2:3 results in an additional boost in current density (blue curve). However, when the $CuCl_2$/MXene ratio is further raised to 2:4, the current density (green curve) sharply declines. Combined with morphological features, it is indicated that the optimal balance of components for maximum electrochemical performance can be achieved at the $CuCl_2$/MXene ratio of 2:3.

Fig. 2(a) and (b) display the detailed morphological structure of Cu-MOF@MXene characterized by SEM. As shown in Fig. 2(a), the homogeneous dispersion of the Cu-MOF@MXene composite decorated on GCE surface is observed. Fig. 2(b) is enlarged from the white square region marked in Fig. 2(a), confirming the detailed structures with Cu-MOF and MXene. The regular octahedral Cu-MOF is interwoven with the MXene fractured layer, enhancing the specific surface area. The surface of MXene is uneven, showing a lamellar, stacked, and tubular structure, whereas Cu-MOF has a smooth surface and adheres to the MXene layers. Fig. 2(c) display the distributions of four elements tested by EDS, illustrating the uniform distributions throughout the composite. The quantitative EDS contents (Fig. S2) is revealed as 43.32% C, 10.25% O, 31.70% F, 3.42% Cl, 7.99% Ti, and 3.32% Cu. The substantial surface area of Cu-MOF@MXene is anticipated to enhance the availability of active sites and improve the adsorption of creatinine molecules. Additionally, the conductive nature of MXene facilitates the electron transfer.

Fig. 2(d) shows the XRD patterns of MXene, Cu-MOF, and Cu-MOF@MXene, within the peak range from 5° to 70°. The black curve represents the characteristic peaks of MXene, with specific angles of

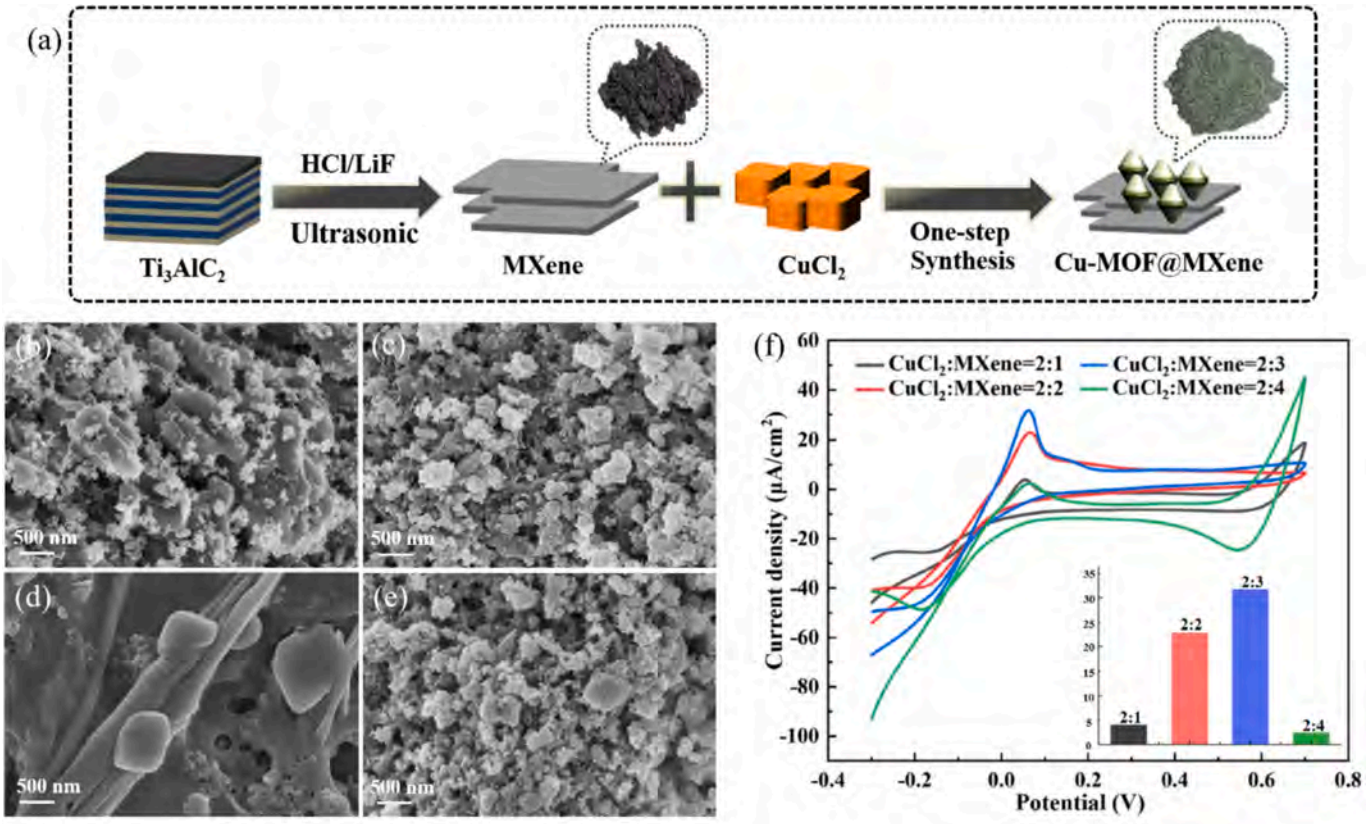

Fig. 1. Morphological changes and electrochemical performance comparison of Cu-MOF@MXene after ratio-optimized preparation. (a) Schematic illustration of the preparation procedure for Cu-MOF@MXene composite; (b)-(e) SEM characterizations of Cu-MOF@MXene with different ratios; (f) CV curves of Cu-MOF@MXene prepared under varying ratios.

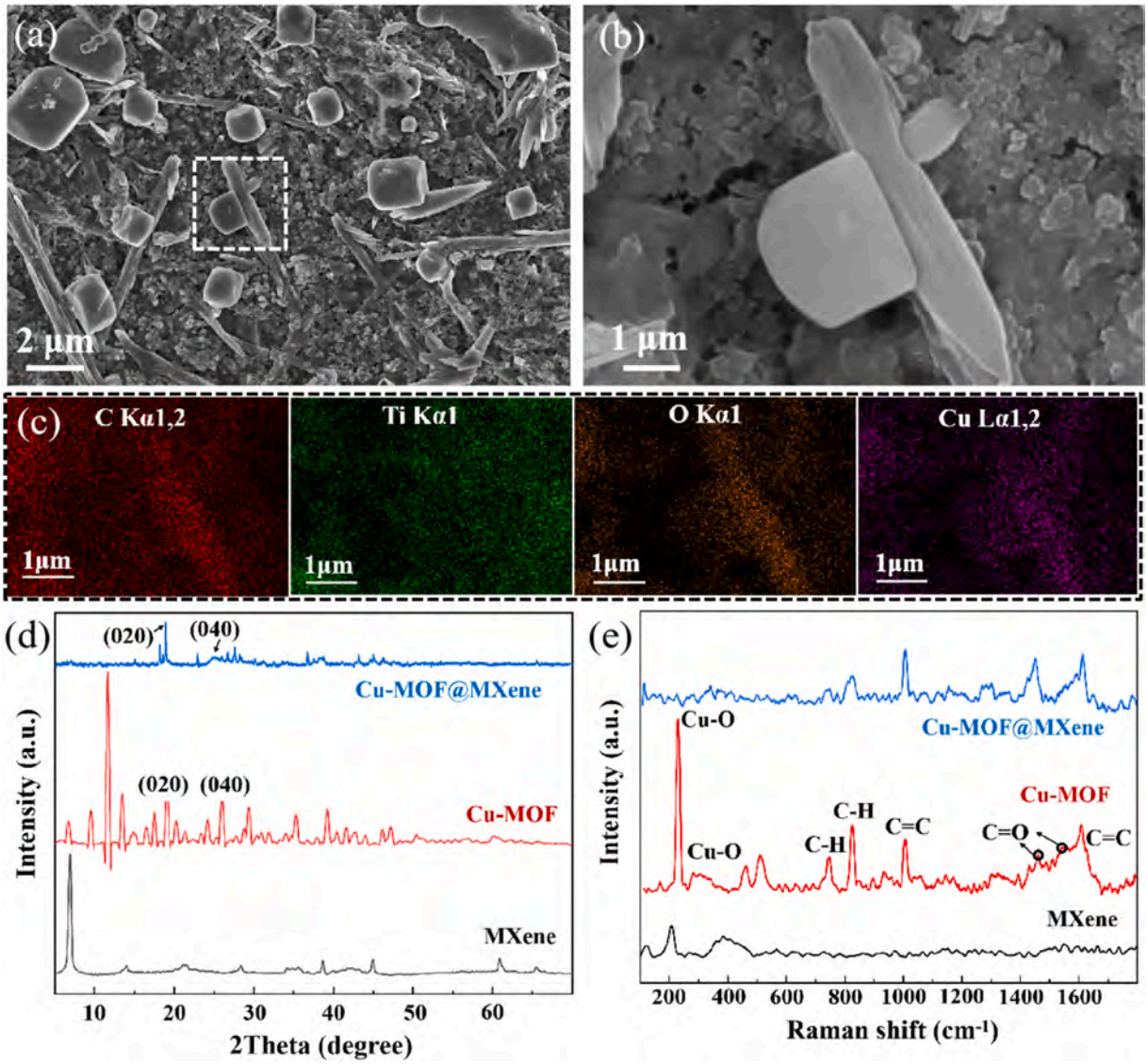

Fig. 2. Material characterization of Cu-MOF@MXene. (a) SEM characterization of Cu-MOF@MXene; (b) Magnified image of (a); (c) EDS results of the quantitative contents of C, Ti, O and Cu; (d) XRD spectra of MXene, Cu-MOF, and Cu-MOF@MXene; (e) Raman spectra of MXene, Cu-MOF, and Cu-MOF@MXene.

6.88°, 14.06°, 21.62°, 28.36°, and 60.82° corresponding to the (002), (004), (006), (008), and (110) crystallographic planes of MXene, respectively [51,52]. The XRD pattern of Cu-MOF reveals the presence of the (020) and (040) planes at 17.3° and 26.8°, respectively [53]. Additionally, the peaks observed at 34.2°, 36.5°, and 41.9° provide evidence for the successful synthesis of crystalline Cu-MOFs [53,54]. To investigate the interactions between Cu-MOF and MXene, XRD analysis is performed on Cu-MOF@MXene, as indicated by the blue curve. The XRD peaks corresponding to the (020) and (040) planes of Cu-MOF are evident [53]. However, the distinctiveness of other Cu-MOF peaks is reduced due to the coating of Cu-MOF on MXene, which blurs some of the peaks. This attenuation can be attributed to the uniform coverage of Cu-MOF on the MXene surface. The integration of MXene into Cu-MOF structure not only influences the crystallographic characteristics, but also suggests potential alterations in the properties [49]. These collective features indicate structural reorganization within the composite, accompanied by reduced crystallinity.

Fig. 2(e) displays the Raman scattering spectra of MXene, Cu-MOF, and Cu-MOF@MXene. The Raman spectrum of MXene (black curve) exhibits major peaks at approximately 150 cm^{-1}, 250 cm^{-1}, 410 cm^{-1} and 600 cm^{-1}, respectively [55]. The peak at 150 cm^{-1} corresponds to the anatase phase of TiO_2, while the other three peaks originate from nonstoichiometric titanium carbide [56]. In the Raman spectrum of Cu-MOF (red curve), the peaks at 235 cm^{-1} and 296 cm^{-1} are attributed to the vibrational modes of Cu—O bonds [57], and the bands at 1463 cm^{-1} and 1551 cm^{-1} are due to the stretching vibration of C═O bonds. The peaks at 1007 and 1614 cm^{-1} indicate the C═C stretching in the benzene rings, while the flexural vibrations of the C—H bond are represented by the peaks at 744 cm^{-1} and 826 cm^{-1} [58]. The Cu-MOF@MXene composite is analyzed to investigate the interactions between Cu-MOF and MXene (blue curve). The C—H, C═C, and C═O bonds of Cu-MOF are consistent with previous results [24,59]. However, the intensity of the Cu—O bond in Cu-MOF decreases somewhat, likely due to the reduction of Cu^{2+} by MXene during the synthesis process. The emergence of peaks specific to MXene at 150 cm^{-1}, 250 cm^{-1}, and 410 cm^{-1} confirms the successful fabrication of the composite.

Fig. 3(a) illustrates the schematics of the preparation, detection process and practical application of the sensor composed of Cu-MOF@MXene. The electrical conductivity of the electrode is enhanced by the Cu-MOF@MXene composite. The complex aggregates on the electrode, resulting in a decrease in the current of Cu/Cu^{2+}. Consequently, the peak current is inversely proportional to the creatinine

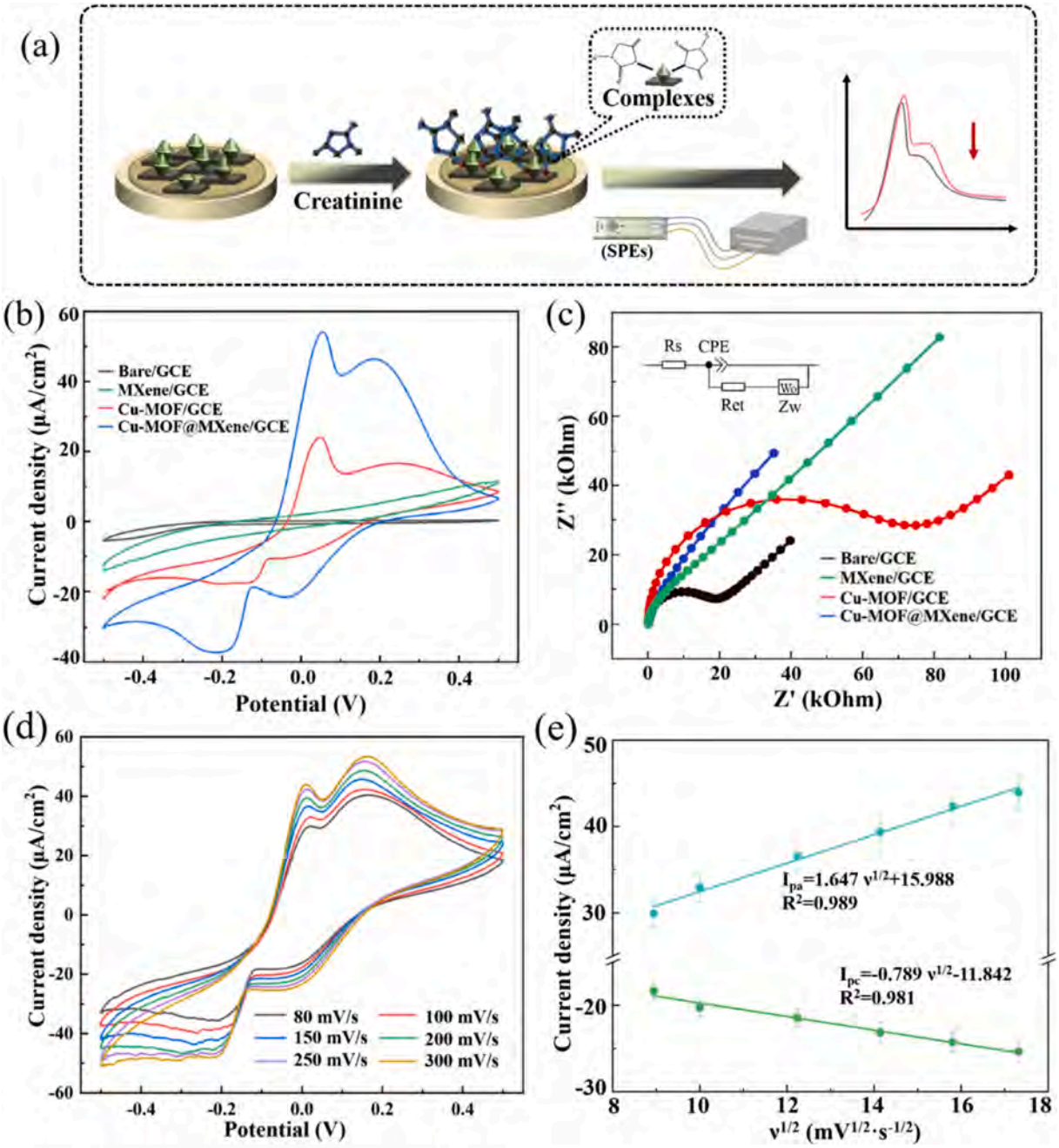

Fig. 3. Electrochemical characterization of electrodes modified with different materials. (a) Schematic of the sensor preparation and detection processes; (b) CV measurements by different electrodes (bare GCE, Cu-MOF/GCE, MXene/GCE, and Cu-MOF@MXene/GCE); (c) EIS measurements by different electrodes; (d) CV curves obtained at different scanning rates of 80 mV/s, 100 mV/s, 150 mV/s, 200 mV/s, 250 mV/s, and 300 mV/s); (e) Linear relationship between the current density and the square root of the scanning rate.

concentration. The detailed mechanism will be elaborated in Fig. 4(a) and (b). Fig. 3(b) presents the CV results of creatinine within a potential range from −0.5 V to +0.5 V at a scanning rate of 50 mV/s in PBS (0.01 M, pH = 7.4). The black, green, red, and blue CV curves correspond to bare GCE, MXene/GCE, Cu-MOF/GCE and Cu-MOF@MXene/GCE, respectively. The electrochemical response observed from the bare GCE (black curve) is relatively weak. However, a notable enhancement in the current density after modifying the GCE with MXene (green curve), suggesting that MXene facilitates electron transfer. The Cu/Cu^{2+} redox couple on the Cu-MOF electrode occurs at an anodic voltage (E_{pa}) of 0.05 V and a cathodic voltage (E_{pc}) of −0.13 V. The electrochemical response of Cu-MOF/GCE (red curve) is much stronger than that of MXene/GCE (green curve). When Cu-MOF@MXene is loaded onto the GCE, an even more pronounced redox reaction of Cu/Cu^{2+} is observed (blue curve). The electrochemical response of Cu-MOF@MXene/GCE is notably superior to that of MXene/GCE due to the inhibited aggregation of MXene nanosheets, which increases the surface area and conductivity. The current response of the Cu-MOF@MXene/GCE (blue curve) is approximately 2.7 times higher than that of the Cu-MOF/GCE (red curve). The increase in the redox current confirms the enhanced electrocatalytic activity of Cu-MOF@MXene/GCE.

EIS is a powerful technique for investigating the impedance characteristics of electrochemical systems. As illustrated in Fig. 3(c), the impedances of the four electrodes (GCE, MXene/GCE, Cu-MOF/GCE and Cu-MOF@MXene/GCE) are derived by fitting the EIS data to an equivalent circuit model. This model comprises the electron transfer

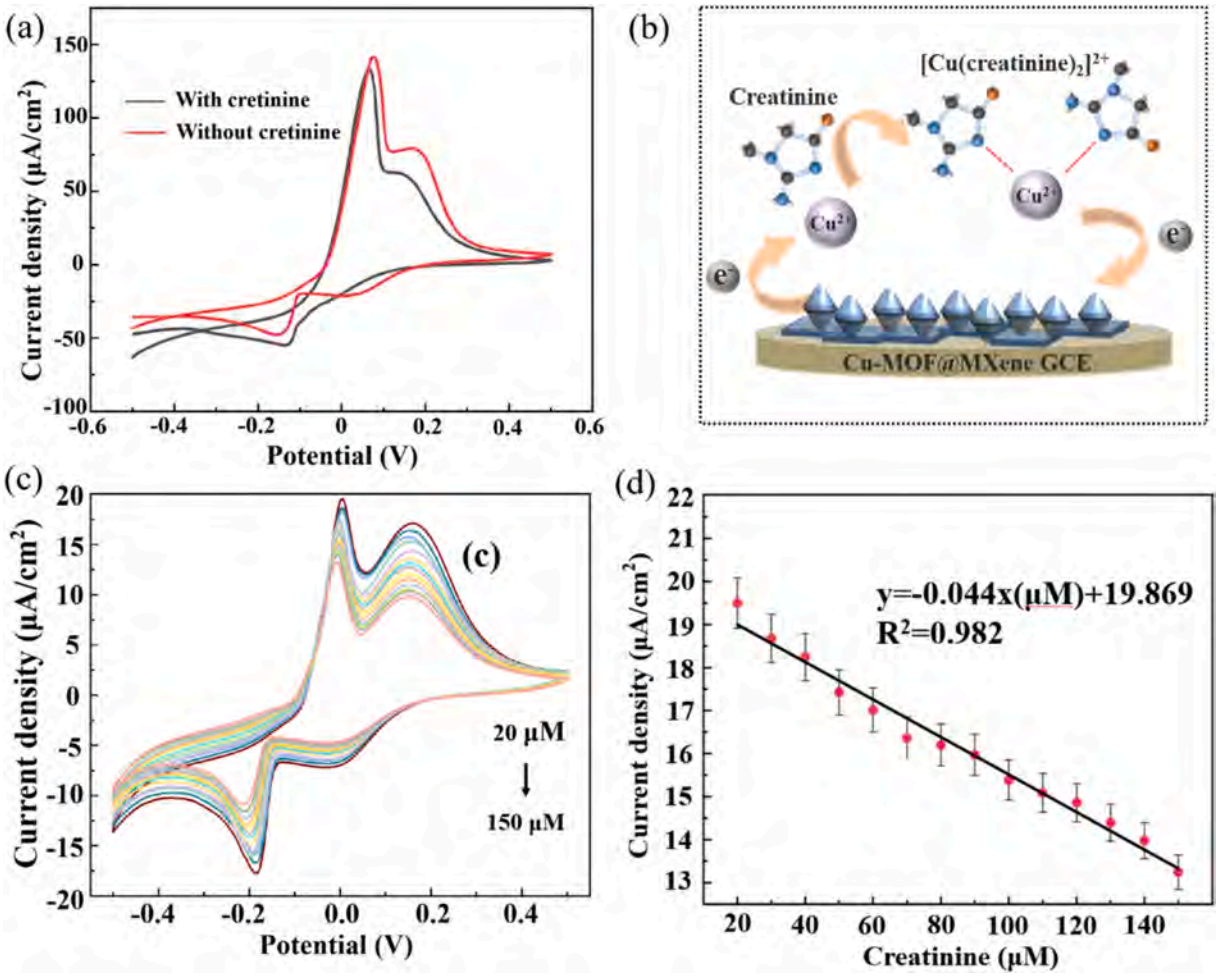

Fig. 4. Schematic diagram of the reaction mechanism at the electrode surface and creatinine concentration detection. (a) Comparison of Cu-MOF@MXene/GCE with and without creatinine; (b) Schematic illustration of the mechanism for the reduction of current densities during CV; (c) Current density versus potential for creatinine concentrations ranging from 20 μM to 150 μM; (d) Linear fitting derived from the data in (c).

resistance (Ret), Warburg impedance (Zw), electrolyte resistance (Rs), and constant phase element (CPE) [60]. Modification with different materials alters Ret due to changes in electrical conductivity. The high-frequency semicircle reflects the electron transfer process, with its diameter equal to the electron transfer resistance [60]. Compared to the bare GCE (black curve), a larger resistance semicircle is observed for Cu-MOF/GCE (red curve), attributed to the inherently poor electrical conductivity of Cu-MOF. When the GCE surface is coated with MXene, the MXene/GCE (green curve) exhibits a smaller resistance due to efficient electron transport facilitated by the metallic elements in MXene. The lattice defects and tunable electronic structure of MXene enhance the electrical conductivity, while surface functional groups and interlayer intercalation further improve the electron migration. After coating GCE with Cu-MOF@MXene, the Cu-MOF@MXene/GCE (blue curve) exhibits an even smaller resistance. This is due to the larger number of electroactive sites on the Cu-MOF@MXene surface, which improves electrical conductivity. EIS and CV produce consistent results, highlighting the enhanced electrochemical properties of Cu-MOF@MXene/GCE.

Fig. 3(d) and (e) evaluate the stability and controllability of Cu-MOF@MXene/GCE. The scanning rate influences the peak current, providing insights into the electrode reactions. CV is performed on Cu-MOF@MXene/GCE at various scanning rates (80 mV/s, 100 mV/s, 150 mV/s, 200 mV/s, 250 mV/s, 300 mV/s). As illustrated in Fig. 3(d), both the anodic peak current density (I_{pa}) and cathodic peak current density (I_{pc}) increase with rising scanning rates, indicating a diffusion-controlled process where the analyte transport rate to the electrode surface determines the current response magnitude. Fig. 3(e) displays the linear relationship between current density and the square root of the scanning rate. The black curve represents the relationship between I_{pa} and the square root of the scanning rate. The linear regression equation is provided as $I_{Pa} = 1.647\nu^{1/2} + 15.988$ with $R^2 = 0.989$. The red curve shows the relationship between I_{pc} and the square root of the scanning rate. The linear regression equation is provided as $I_{Pc} = -0.789\nu^{1/2} - 11.842$ with $R^2 = 0.981$. Both equations exhibit the good linearity, demonstrating an ideal and stable diffusion-controlled process.

Fig. 4(a) depicts the difference between Cu-MOF@MXene/GCE in the presence and absence of creatinine. Notably, when creatinine is introduced, the peak current associated with Cu/Cu^{2+} redox pair decreases. Fig. 4(b) elucidates the mechanism underlying the reduction in current density. Typically, the interaction between creatinine molecules and Cu^{2+} within Cu-MOF@MXene is facilitated by the strong electrostatic attraction between the nitrogen-containing groups of creatinine and the active metal sites [61]. This interaction gives rise to the formation and subsequent adsorption of creatinine-metal (copper) complexes on the electrode surface. As a result, the number of available active sites for the Cu/Cu^{2+} redox pair is reduced [31]. Consequently, the accumulation of creatinine-metal complexes leads to a decrease in the effective electroactive surface area and, accordingly the signal intensity. The affinity between creatinine molecules and metal ions plays a critical role in quantitative determination [30].

The processes occurring on the electrode in the absence and presence

of creatinine can be described as follows [61]:

In the absence of creatinine:

$$Cu_{(s)} \rightarrow Cu^{2+}_{(aq)} + 2e^- \quad (1)$$

$$Cu^{2+}_{(aq)} + 2e^- \rightarrow Cu_{(s)} \quad (2)$$

In the presence of creatinine:

$$Cu_{(s)} + 2creatinine \rightarrow \left[Cu(creatinine)_2\right]^{2+}(aq) + 2e^- \quad (3)$$

$$\left[Cu(creatinine)_2\right]^{2+}(aq) + 2creatinine(aq) + e^- \rightarrow \left[Cu(creatinine)_4\right]^{+}(aq) \quad (4)$$

As depicted in Fig. 4(b), when a potential is applied, oxidation takes places on Cu-MOF@MXene/GCE, leading to the generation of Cu^{2+} ions. Subsequently, the nitrogen-containing core of creatinine undergoes self-assembly with Cu^{2+} ions derived from the Cu-MOF@MXene and attaches to the electrode, forming a creatinine-Cu^{2+} complex. This process results in a decrease in the concentration of freely available Cu^{2+} ions and a corresponding modulation of the current density, which varies in accordance with the creatinine concentration.

The redox activity of Cu-MOF@MXene/GCE can be demonstrated by the CV method. Fig. 4(c) displays the CV results to depict the relationship between current density and potential for various creatinine concentrations. The creatinine concentrations are varied between 20 μM and 150 μM, specifically at 20 μM, 30 μM, 40 μM, 50 μM, 60 μM, 70 μM, 80 μM, 90 μM, 100 μM, 110 μM, 120 μM, 130 μM, 140 μM, and 150 μM. The 3D waterfall chart (Fig. S3) can elucidate the relationship between the current density, creatinine concentration, and time. Cu-MOF@MXene/GCE exhibits a sensitive current response upon the addition of creatinine. The peak current, occurring within the range of 9.91 s to 10.15 s, is associated with the Cu/Cu^{2+} redox pair and decreases with increasing creatinine concentration. The peak current of Cu-MOF@MXene/GCE, spanning from −7.6 mV to +4.3 mV, also diminishes as the creatinine concentration increases.

The sensing mechanism is as follows:

Peak 1 (~ −0.05 V): Partial oxidation of $Cu^0 \rightarrow Cu^+$.

Peak 2 (~ +0.15 V): Complete oxidation of $Cu^+ \rightarrow Cu^{2+}$.

Peaks 3/4: Redox reactions involving oxygen-containing functional groups (-OH/-O) on MXene.

Fig. 4(d) exhibits the linear relationship between creatinine concentration and current response, based on the 14 data points in Fig. 4(c). This peak, occurring in ~−0.05 V, decreases with increasing creatinine concentration, as shown in Fig. 4(c). The corresponding linear regression equation is provided as $I_p(\mu A) = -0.044x(\mu M) + 19.869$ with $R^2 = 0.982$. The calibration diagram demonstrates a good linear relationship, indicating the potential for practical detectionl. The LOD for creatinine is calculated to be 20.069 μM($N = 3$, STDEV = 0.321 μM), using the formula of $LOD = m + S/N \times b$, where m represents the slope of the linear regression equation, S/N is the signal-to-noise ratio (SNR = 3), and b is the background noise (0.1 μM).

Compared with other copper-based nanomaterials, the Cu-MOF employed in this study demonstrates unique advantages for electrochemical creatinine detection. In contrast to conventional copper nanoparticles and copper oxide materials, Cu-MOF significantly enhances sensor sensitivity due to its larger specific surface area and more abundant active sites. Meanwhile, its well-ordered porous structure not only effectively prevents the aggregation of active sites but also improves detection selectivity through precise molecular sieving effects. Furthermore, the inherent structural stability of Cu-MOF enables it to maintain excellent performance over multiple testing cycles. These characteristics endow the material with greater potential for practical applications [62].

Fig. 6 compares the sensing performance of reported creatinine sensors, highlighting that the Cu-MOF@MXene sensor outperforms the other reported ones in terms of sensitivity within the effective linear range. Although the linear detection range is relatively narrow, our sensor has demonstrated excellent performance in terms of sensitivity, selectivity, and stability. It has a high sensitivity and a low detection limit (20.069 μM), which are sufficient to meet the requirements of most clinical detections. In the detection of real urine and serum samples, the sensor is able to accurately detect creatinine concentration through appropriate preprocessing steps.

The electrochemical effectiveness of creatinine detection is further explored through CA technique under continuous stirring. This technique optimizes mass transfer by stirring and also increases the sampling time, with the noise being within the controllable range. Compared with the conventional CV/EIS techniques, CA technique is applicable for rapid response detection. Fig. 5 evaluates the sensitivity and selectivity of Cu-MOF@MXene/GCE. Fig. 5(a) depicts the current response of Cu-MOF@MXene/GCE during the successive addition of creatinine along with other potential interferences, namely ascorbic acid (AA), uric acid (UA), glucose (Glu), and urea. Upon the addition of creatinine, Cu-MOF@MXene/GCE exhibits a decreased current density. In the contrast, the current responses to other potential interfering substances remain minimal. Fig. 5(b) illustrates the percentage relationships between the current responses triggered by the interferences and creatinine. The percentage decrease in the current density ($\Delta I_{Cre}/\Delta I_{Cre}$) triggered by the addition of creatinine is defined as 100%. The percentages of the current density decreases triggered by AA, UA, Glu and urea ($\Delta I_{AA}/\Delta I_{Cre}$, $\Delta I_{UA}/\Delta I_{Cre}$, $\Delta I_{Glu}/\Delta I_{Cre}$, and $\Delta I_{Uera}/\Delta I_{Cre}$) are calculated to be 11.60%, 3.75%, 12.50%, and 5.00%, respectively. Although the response values of AA and Glu are slightly higher, compared with other interferents, their impact is still within the controllable range. In the detection of real urine and serum samples, the sensor shows high accuracy and stability in detecting creatinine, indicating that even in the presence of these interferents, the sensor can still reliably detect creatinine. Such selectivity is highly promising for the analysis of complex biological samples. While these results confirm the sensor's robustness in typical biological environments, we recognize that certain medications (e.g., antibiotics) or pathological metabolites may require additional evaluation. Nevertheless, the successful quantification in pretreated human samples (Section 2.7) with clinically acceptable accuracy validates the current methodology. A more extensive interference study will be conducted in subsequent research to address specialized clinical scenarios.

In Fig. 5(c), the I-t curve of the response current of Cu-MOF@MXene/GCE upon successive additions of creatinine. The creatinine solution (1.0 μM) is continuously injected into a stirred PBS solution (0.01 M). The current response of Cu-MOF@MXene/GCE attains a steady state within 1 s after the injection of the creatinine solution. This attainment of the steady state demonstrates the sensor's rapid response characteristic and high sensitivity. The stability and reliability of Cu-MOF@MXene/GCE are evaluated in triplicate experiments by SPE. The SPE consists of an electrochemical three-electrode system, wherein the reference electrode is Ag/AgCl, and the counter electrode is made of platinum. Fig. 5(d) presents the stability data obtained from three consecutive tests. When compared with the first test, the value obtained in the second test is 96.8% of the initial value, and in the third test, it decreases to 92.7% of the initial value. These results indicate the good stability of Cu-MOF@MXene. The Cu-MOF@MXene sensor demonstrated excellent long-term stability in simulated biological fluid (0.01 M PBS + 0.1 M NaCl, pH 7.4), maintaining consistent current responses with only 1.6–2.4% variation during 5-day accelerated aging tests (Fig. S5). The results confirm reliable operation within typical clinical detection timeframes, while further studies under extended conditions remain valuable for comprehensive evaluation.

Recovery experiments are carried out using the SPE with the Cu-MOF@MXene composite to evaluate its performance in detecting creatinine in human urine samples. Various concentrations of creatinine solutions are added to simulate the real samples, and the recovery rate is

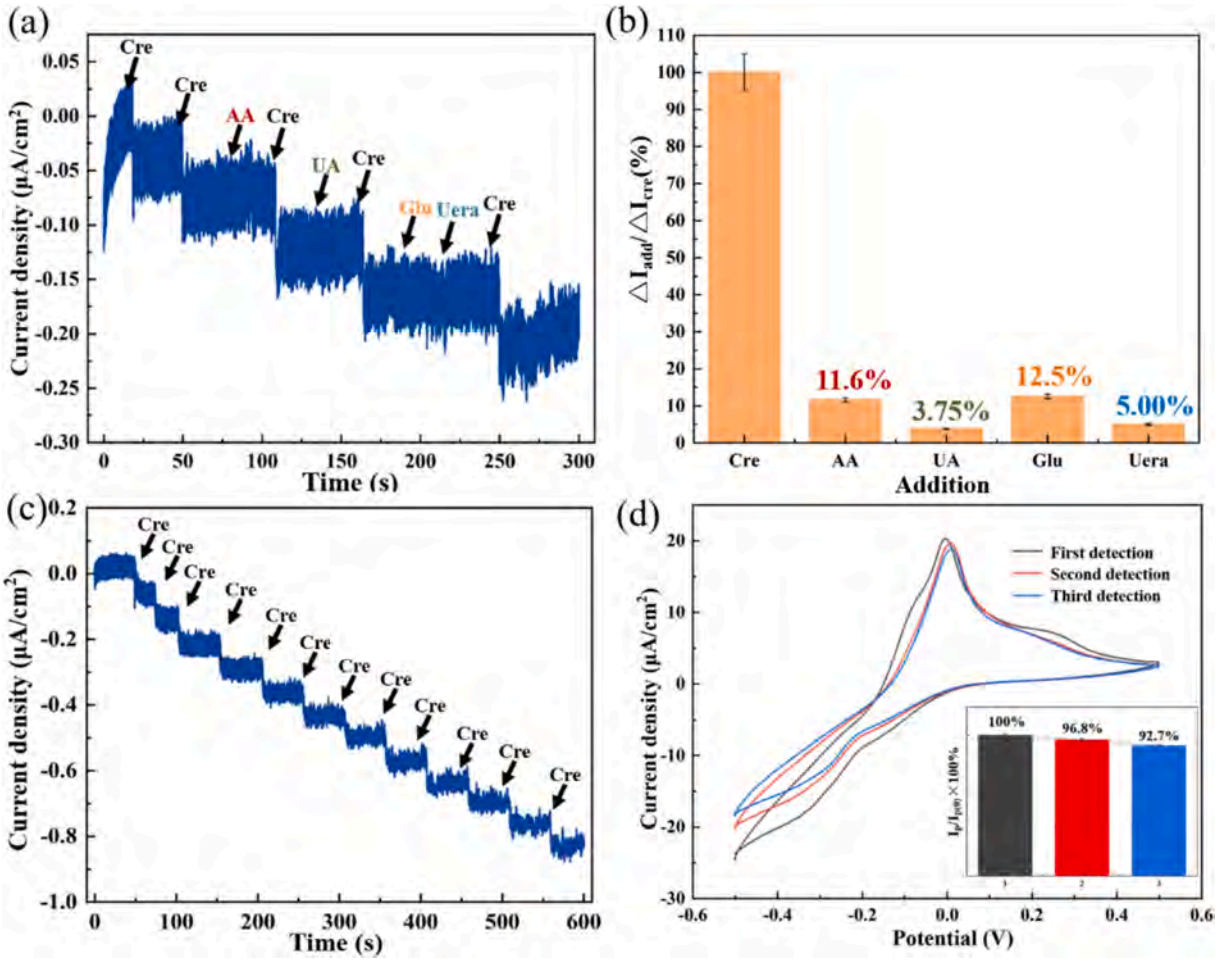

Fig. 5. Sensitivity and selectivity of Cu-MOF@MXene/GCE evaluated by CA, (a) Current densities for successive additions of interferences and creatinine; (b) Current response percentages for interferences and creatinine; (c) I-t curve for successive additions of creatinine; (d) Stability and reproducibility of the SPE with Cu-MOF@MXene over multiple assessments.

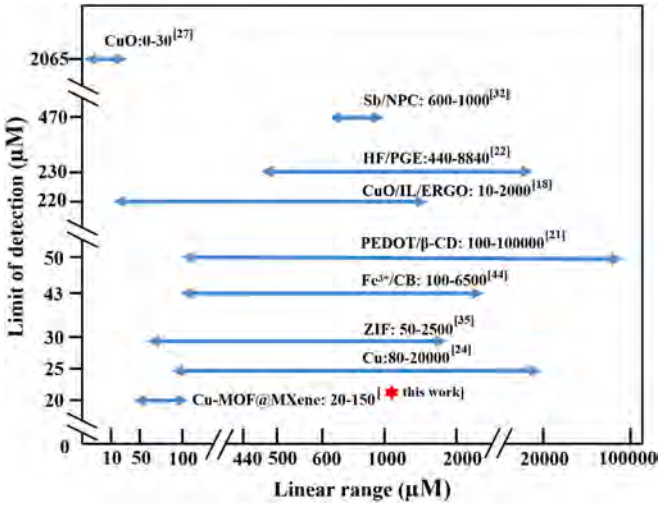

Fig. 6. Comparison of statistical data between this work and previously reported references.

calculated as the ratio of the added creatinine to the detected amout. Fig. 7(a) demonstrates that the recovery rates for human urine samples ranges from 97.2% to 104.0%, indicating a high level of accuracy. To further assess the clinical applicability, a comparative evaluation is presented in Fig. 7(b). This evaluation utilizes randomly selected serum samples with known creatinine concentrations as references. The standard creatinine concentration are pre-measured using a clinical enzymatic method. The creatinine concentrations are then calculated using the linear regression equation shown in Fig. 4(c). The results show a good agreement with the tandard values, with deviations ranging from 0.8% and 13.3%, thereby confirming the accuracy of creatinine detection.

4. Conclusions

In this study, Cu-MOF@MXene is synthesized through a cost-effective one-step process using available reactive precursors. This composite material exhibits unique structural and performance advantages, making it highly suitable for nonenzymatic electrochemical sensing of creatinine. The Cu-MOF@MXene retains the high specific surface area and porous structure characteristic of MOFs, while also incorporating the 2D layered properties of MXene. The 3D architecture of Cu-MOF enhances the material's adsorption capacity, and the MXene layers contribute to increased conductivity, thereby improving the electrochemical performance for creatinine detection. The Cu-MOF@MXene electrode demonstrates a favorable linear range (20.0 μM to 150.0 μM) and a low LOD (20.069 μM, $N = 3$). The electrochemical properties of Cu-MOF@MXene surpass those of both Cu-MOF and MXene alone. Furthermore, a SPE coated with Cu-MOF@MXene is successfully fabricated and employed for detection of creatinine in both urine and human serum samples. The SPE benefits from the high

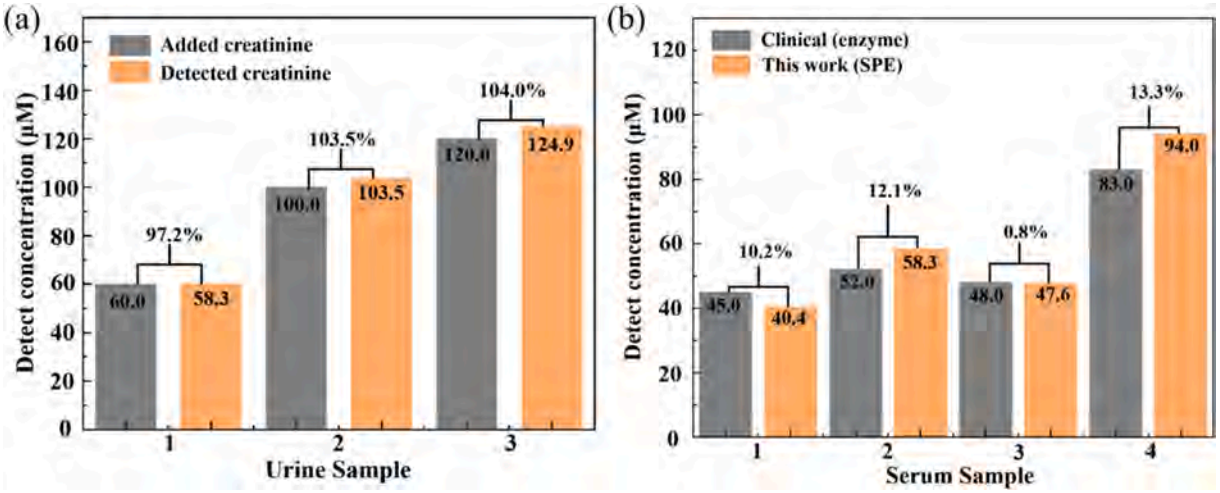

Fig. 7. Analysis of real samples using SPEs (a) Recovery rates of creatinine detection in human urine samples using the SPE method; (b) Creatinine concentrations in four serum samples detected by the clinical method and SPE.

electrical conductivity, good stability, and selectivity of Cu-MOF@MXene, showcasing high sensitivity, selectivity, and reproducibility in the electrochemical detection of creatinine. These attributes enable accurate detection of creatinine in complex biological samples, even in the presnece of other interfering substances. This study not only introduces a cost-effective approach for synthesizing composite materials but also provides valuable insights and references for the advancement of high-performance biosensors in clinical and medical diagnostics.

CRediT authorship contribution statement

Xianglong Bian: Writing – original draft, Methodology, Investigation, Formal analysis, Data curation, Conceptualization. **Dong Yang:** Writing – review & editing, Software, Formal analysis. **Lin Chen:** Methodology. **Yingfei Zeng:** Investigation. **Li Zhu:** Investigation. **Hua Pei:** Validation, Resources, Methodology, Formal analysis. **Qianfeng Xia:** Supervision. **Paul K. Chu:** Writing – review & editing, Funding acquisition, Formal analysis. **Tingwei Hu:** Writing – review & editing, Supervision, Project administration, Funding acquisition, Formal analysis, Data curation, Conceptualization.

Ethics approval and consent to participate

During the study, we strictly followed the principle of informed consent. We clearly communicated the study's purpose, procedures, risks, and benefits to all participants, either verbally or in writing, and obtained their consent. Participants were informed that their participation was voluntary and that they could withdraw at any time. We also prioritized patient privacy by anonymizing all serum samples to prevent identification and protect privacy rights.

Funding

This work was jointly supported by the Hainan Provincial Natural Science Foundation of China (No. 521RC555), Special Talent Researching Funds (RZ2500001778, RC2400001279, XRC200016), and City University of Hong Kong Donation Research Grants (DON-RMG 9229021 and 9220061).

Declaration of competing interest

The authors declare that they have no known competing financial interests or personal relationships that could have appeared to influence the work reported in this paper.

Appendix A. Supplementary data

Supplementary data to this article can be found online at https://doi.org/10.1016/j.microc.2025.114915.

Data availability

Data will be made available on request.

References

[1] K. Kashani, M.H. Rosner, M. Ostermann, Creatinine: from physiology to clinical application, Eur. J. Intern. Med. 72 (2020) 9–14, https://doi.org/10.1016/j.ejim.2019.10.025.
[2] C.S. Pundir, P. Kumar, R. Jaiwal, Biosensing methods for determination of creatinine: a review, Biosens. Bioelectron. 126 (2019) 707–724, https://doi.org/10.1016/j.bios.2018.11.031.
[3] H. Pottel, J. Björk, U. Nyman, P. Delanaye, Development and validation of a modified full age spectrum creatinine-based equation to estimate glomerular filtration rate, Ann. Intern. Med. 174 (2021) 183–191, https://doi.org/10.7326/m20-4366.
[4] K. Kalantar-Zadeh, T.H. Jafar, D. Nitsch, B.L. Neuen, V. Perkovic, Chronic kidney disease, Lancet 398 (2021) 786–802, https://doi.org/10.1016/s0140-6736(21)00519-5.
[5] K. Boss, S. Stolpe, A. Müller, B. Wagner, M. Wichert, R. Assert, L. Volbracht, A. Stang, B. Kowall, A. Kribben, Effect of serum creatinine difference between the Jaffe and the enzymatic method on kidney disease detection and staging, Clin. Kidney J. 16 (2023) 2147–2155, https://doi.org/10.1093/ckj/sfad178.
[6] I.B. Linnet Kristian, HPLC with enzymatic detection as a candidate reference method for serum creatinine, Clin. Chem. 37 (1991) 1669–1675.
[7] J. Li, Z. Li, Y. Dou, J. Su, J. Shi, Y. Zhou, L. Wang, S. Song, C. Fan, A nano-integrated microfluidic biochip for enzyme-based point-of-care detection of creatinine, Chem. Commun. 57 (2021) 4726–4729, https://doi.org/10.1039/d1cc00825k.
[8] D. Lakshmi, B.B. Prasad, P.S. Sharma, Creatinine sensor based on a molecularly imprinted polymer-modified hanging mercury drop electrode, Talanta 70 (2006) 272–280, https://doi.org/10.1016/j.talanta.2006.02.038.
[9] H. Hou, Y. Liu, X. Li, W. Liu, X. Gong, Rapid electrodeposition of cu nanoparticle film on Ni foam as an integrated 3D free-standing electrode for non-invasive and non-enzymatic creatinine sensing, Analyst 149 (2024) 2905–2914, https://doi.org/10.1039/d4an00162a.
[10] S. Yadav, R. Devi, P. Bhar, S. Singhla, C.S. Pundir, Immobilization of creatininase, creatinase and sarcosine oxidase on iron oxide nanoparticles/chitosan-g-polyaniline modified Pt electrode for detection of creatinine, Enzym. Microb. Technol. 50 (2012) 247–254, https://doi.org/10.1016/j.enzmictec.2012.01.008.
[11] J.G.H. Cook, Factors influencing the assay of creatinine, Ann. Clin. Biochem. 12 (1975) 219–232.
[12] W. Greg Miller, G.L. Myers, Edward R. Ashwood, Lothar Siekmann, Creatinine measurement state of the art in accuracy and interlaboratory harmonization, Arch. Pathol. Lab Med. 129 (2005) 297–304.

[13] H. Beitollahi, Z. Sarbandian, An electrochemical sensor based on a modified glassy carbon electrode for detection of epinephrine in the presence of theophylline, Admet. Dmpk. 12 (2024) 391–402, https://doi.org/10.5599/admet.2082.

[14] P. Mohammadzadeh Jahani, R. Zaimbashi, M.R. Aflatoonian, S. Tajik, H. Beitollahi, Electrochemical sensor for acetylcholine detection based on WO_3 nanorods-modified glassy carbon electrode, J. Electrochem. Sci. Eng. 14 (2024) 631–641, https://doi.org/10.5599/jese.2462.

[15] P. Mohammadzadeh Jahani, R. Khorramdel Sharfooei Nejad, R. Zaimbashi, F. Garkani Nejad, S.Z. Moammadi, S. Tajik, H. Beitollahi, A voltammetric sensor based on $CuCo_2O_4$ nanorods and ionic liquid for determination of sunset yellow, J. Electrochem. Sci. Eng. 14 (2024) 643–652, https://doi.org/10.5599/jese.2484.

[16] E.L. Fava, T.M.d. Prado, A. Garcia-Filho, T.A. Silva, F.H. Cincotto, F. Cruz de Moraes, R.C. Faria, O. Fatibello-Filho, Non-enzymatic electrochemical determination of creatinine using a novel screen-printed microcell, Talanta 207 (2020), https://doi.org/10.1016/j.talanta.2019.120277.

[17] U. Amara, I. Hussain, M. Ahmad, K. Mahmood, K. Zhang, 2D MXene-based biosensing: a review, Small 19 (2022) 2205249–2205287, https://doi.org/10.1002/smll.202205249.

[18] S. Boobphahom, N. Ruecha, N. Rodthongkum, O. Chailapakul, V.T. Remcho, A copper oxide-ionic liquid/reduced graphene oxide composite sensor enabled by digital dispensing: non-enzymatic paper-based microfluidic determination of creatinine in human blood serum, Anal. Chim. Acta 1083 (2019) 110–118, https://doi.org/10.1016/j.aca.2019.07.029.

[19] P. Singh, S. Mandal, D. Roy, N. Chanda, Facile detection of blood creatinine using binary copper–iron oxide and rGO-based nanocomposite on 3D printed Ag-electrode under POC settings, ACS Biomater Sci. Eng. 7 (2021) 3446–3458, https://doi.org/10.1021/acsbiomaterials.1c00484.

[20] R. Cánovas, M. Cuartero, G.A. Crespo, Modern creatinine (bio)sensing: challenges of point-of-care platforms, Bionsens. Bioelectron. 130 (2019) 110–124, https://doi.org/10.1016/j.bios.2019.01.048.

[21] Kumar, T. Naresh, A. Ananthi, J. Mathiyarasu, J. Joseph, K. Lakshminarasimha Phani, V. Yegnaraman, Enzymeless creatinine estimation using poly (3,4-ethylenedioxythiophene)-β-cyclodextrin, J. Electroanal. Chem. 661 (2011) 303–308, https://doi.org/10.1016/j.jelechem.2011.08.001.

[22] S. Hooshmand, Z. Es'haghi, Microfabricated disposable nanosensor based on CdSe quantum dot/ionic liquid-mediated hollow fiber-pencil graphite electrode for simultaneous electrochemical quantification of uric acid and creatinine in human samples, Anal. Chim. Acta 972 (2017) 28–37, https://doi.org/10.1016/j.aca.2017.04.035.

[23] A.L. Ferguson, J. Hachmann, T.F. Miller, J. Pfaendtner, The journal of physical chemistry A/B/C virtual special issue on machine learning in physical chemistry, J. Phys. Chem. C 124 (2020) 24033–24038, https://doi.org/10.1021/acs.jpcc.0c09208.

[24] P. Ming, Y. Niu, Y. Liu, J. Wang, H. Lai, Q. Zhou, H. Zhai, An electrochemical sensor based on Cu-MOF-199@MWCNTs laden with CuNPs for the sensitive detection of creatinine, Langmuir 39 (2023) 13656–13667, https://doi.org/10.1021/acs.langmuir.3c01823.

[25] A. Nagarajan, V. Sethuraman, R. Sasikumar, Non-enzymatic electrochemical detection of creatinine based on a glassy carbon electrode modified with a Pd/Cu_2O decorated Polypyrrole (PPy) nanocomposite: an analytical approach, Anal. Methods 15 (2023) 1410–1421, https://doi.org/10.1039/d3ay00110e.

[26] I.S. Kucherenko, O.O. Soldatkin, S.V. Dzyadevych, A.P. Soldatkin, Electrochemical biosensors based on multienzyme systems: main groups, advantages and limitations- a review, Anal. Chim. Acta 1111 (2020) 114–131, https://doi.org/10.1016/j.aca.2020.03.034.

[27] T. Hongboontry, S. Ponwaranon, S. Sirijongdee, C. Thanachayanont, P. Pungetmongkol, Low-cost and portable creatinine electrochemical sensor for non-invasive chronic kidney disease monitoring, Nano (2021) 159–162, https://doi.org/10.1109/nano51122.2021.9514318.

[28] P.R.M. Krishnan, A. Sakthivel, S. Alwarappan, Sulfur doped graphitic carbon nitride Nanosheets for the electrochemical detection of DNA bases, J. Electrochem. Soc. 170 (2023), https://doi.org/10.1149/1945-7111/acfa82.

[29] A.E. Subbiah Alwarappan, Chang Liu, Chen-Zhong Li, Probing the electrochemical properties of graphene nanosheets for biosensing applications, J. Phys. Chem. C 113 (2009) 8853–8857.

[30] S. Jankhunthod, K. Kaewket, P. Termsombut, C. Khamdang, K. Ngamchuea, Electrodeposited copper nanoparticles for creatinine detection via the in situ formation of copper-creatinine complexes, Anal. Bioanal. Chem. 415 (2023) 3231–3242, https://doi.org/10.1007/s00216-023-04699-3.

[31] X. Gao, R. Gui, H. Guo, Z. Wang, Q. Liu, Creatinine-induced specific signal responses and enzymeless ratiometric electrochemical detection based on cpper nanoparticles electrodeposited on reduced graphene oxide-based hybrids, Sensors Actuators B Chem. 285 (2019) 201–208, https://doi.org/10.1016/j.snb.2019.01.057.

[32] M. Jamil, B. Fatima, M.N. Ashiq, M. Najam-ul-Haq, Quantitative determination of creatinine from serum of prostate cancer patients by N-doped porous carbon antimony (Sb/NPC) nanoparticles, Bioelectrochemistry 140 (2021) 1–8, https://doi.org/10.1016/j.bioelechem.2021.107815.

[33] S. Jin, How to effectively utilize MOFs for electrocatalysis, ACS Energy Lett. 4 (2019) 1443–1445, https://doi.org/10.1021/acsenergylett.9b01134.

[34] C. Soosaimanickam, K. Murugavel, S. Alwarappan, Bimetallic MOFs-based electrodes for the simultaneous electrochemical detection of epinephrine and norepinephrine, J. Electrochem. Soc. 171 (2024), https://doi.org/10.1149/1945-7111/ad6c80.

[35] T. Chakraborty, M. Das, C. Lin, Y. Su, B. Yuan, C.-H. Kao, ZIF-8 nanoparticles based electrochemical sensor for non-enzymatic creatinine detection, Membranes 12 (2022) 159–173, https://doi.org/10.3390/membranes12020159.

[36] C. Soosaimanickam, A. Sakthivel, K. Murugavel, S. Alwarappan, Zeolite Imidazolate framework-based platform for the electrochemical detection of epinephrine, J. Electrochem. Soc. 170 (2023), https://doi.org/10.1149/1945-7111/acff21.

[37] J. Wang, Q. Xu, Y. Yang, J. Liu, W. Kong, L. Shi, An electrochemical sensor founded on heterogeneous MXene & MOF composite for tanshinol sensing, Talanta 268 (2024) 125344–125351, https://doi.org/10.1016/j.talanta.2023.125344.

[38] L. Qu, M. Wu, L. Zhao, J. Li, H. Pan, A sandwich electrochemical immunosensor based on MXene@dual MOFs for detection of tumor marker CA125, Microchim. Acta 190 (2023) 1–10, https://doi.org/10.1007/s00604-023-05719-w.

[39] H. Wang, L. Cai, Y. Wang, C. Liu, G. Fang, S. Wang, Covalent molecularly imprinted electrochemical sensor modulated by borate ester bonds for Hygromycin B detection based on the synergistic signal amplification of Cu-MOF and MXene, Food Chem. 383 (2022) 132382–132389, https://doi.org/10.1016/j.foodchem.2022.132382.

[40] Y. Qi, Y. Chen, Q. Li, X. Dang, H. Chen, A novel ratiometric electrochemical sensing platform combined with molecularly imprinted polymer and Fe-MOF-NH_2/CNTs-NH_2/MXene composite for efficient detection of ofloxacin, Anal. Chim. Acta 1316 (2024) 342876–342884, https://doi.org/10.1016/j.aca.2024.342876.

[41] D. Song, X. Jiang, Y. Li, X. Lu, S. Luan, Y. Wang, Y. Li, F. Gao, Metal-organic frameworks-derived MnO_2/Mn_3O_4 microcuboids with hierarchically ordered nanosheets and Ti_3C_2 MXene/AuNPs composites for electrochemical pesticide detection, J. Hazard. Mater. 373 (2019) 367–376, https://doi.org/10.1016/j.jhazmat.2019.03.083.

[42] A. VahidMohammadi, J. Rosen, Y. Gogotsi, The world of two-dimensional carbides and nitrides (MXenes), Science 372 (2021) 1–14, https://doi.org/10.1126/science.abf1581.

[43] Q. Zhou, L. Wang, H. Zheng, Z. Peng, Z. Hu, Y. Zhou, B. Wang, An ultrasensitive MXene-based electrochemical immunosensor for the detection and species identification of archaeological silk microtraces, Biosens. Bioelectron. 238 (2023) 115581–115589, https://doi.org/10.1016/j.bios.2023.115581.

[44] Z. Yang, A. Liu, C. Wang, F. Liu, J. He, S. Li, J. Wang, R. You, X. Yan, P. Sun, Y. Duan, G. Lu, Improvement of gas and humidity sensing properties of organ-like MXene by alkaline treatment, ACS Sens. 4 (2019) 1261–1269, https://doi.org/10.1021/acssensors.9b00127.

[45] S. Alwarappan, N. Nesakumar, D. Sun, T.Y. Hu, C.-Z. Li, 2D metal carbides and nitrides (MXenes) for sensors and biosensors, Biosens. Bioelectron. 205 (2022), https://doi.org/10.1016/j.bios.2021.113943.

[46] W. Liu, S. Kang, Q. Zhang, S. Chen, Q. Yang, B. Yan, Self-assembly fabrication of chitosan-tannic acid/MXene composite film with excellent antibacterial and antioxidant properties for fruit preservation, Food Chem. 410 (2023) 135405, https://doi.org/10.1016/j.foodchem.2023.135405.

[47] D. Parajuli, N. Murali, K. C D, B. Karki, K. Samatha, A.A. Kim, M. Park, B. Pant, Advancements in MXene-polymer nanocomposites in energy storage and biomedical applications, Polymers 14 (2022) 1–41, https://doi.org/10.3390/polym14163433.

[48] X. Bian, D. Yang, Y. Zeng, T. Yang, Q. Xia, T. Hu, High electrochemical performance of glucose detection based on tapered gold nanostructures and MXene layers, Sens. Actuator Rep. 8 (2024) 100232–100244, https://doi.org/10.1016/j.snr.2024.100232.

[49] C. Liu, Y. Bai, W. Li, F. Yang, G. Zhang, H. Pang, In situ growth of three-dimensional MXene/metal-organic framework composites for high-performance supercapacitors, Angew. Chem. Int. Ed. 61 (2022) 1–7, https://doi.org/10.1002/anie.202116282.

[50] E.L. Fava, T.M.d. Prado, A. Garcia-Filho, T.A. Silva, F.H. Cincotto, F. Cruz de Moraes, R.C. Faria, O. Fatibello-Filho, Non-enzymatic electrochemical determination of creatinine using a novel screen-printed microcell, Talanta 207 (2020) 120277–120282, https://doi.org/10.1016/j.talanta.2019.120277.

[51] Z. Pan, F. Cao, X. Hu, X. Ji, A facile method for synthesizing CuS decorated Ti_3C_2 MXene with enhanced performance for asymmetric supercapacitors, J Mater Chem A 7 (2019) 8984–8992, https://doi.org/10.1039/c9ta00085b.

[52] W. Feng, H. Luo, Y. Wang, S. Zeng, L. Deng, X. Zhou, H. Zhang, S. Peng, Ti_3C_2 MXene: a promising microwave absorbing material, RSC Adv. 8 (2018) 2398–2403, https://doi.org/10.1039/c7ra12616f.

[53] M. Zhong, S. Zhang, A. Dong, Z. Sui, L. Feng, Q. Chen, Cu-MOF/Au–Pd composite catalyst: preparation and catalytic performance evaluation, J. Mater. Sci. 55 (2020) 10388–10398, https://doi.org/10.1007/s10853-020-04699-z.

[54] A.H. Shah, Z.U. Abideen, S. Maqsood, F. Rashid, R. Ullah, A.U. Rehman, M. Dildar, M. Ahmad, K. Ullah, M.N. Rafi, F. Teng, Porous cu-based metal organic framework (Cu-MOF) for highly selective adsorption of organic pollutants, J. Solid State Chem. 322 (2023) 123935–123945, https://doi.org/10.1016/j.jssc.2023.123935.

[55] K.J. Cai, Y. Zheng, P. Shen, S.Y. Chen, TiC_x–Ti_2C nanocrystals and epitaxial graphene-based lamellae by pulsed laser ablation of bulk TiC in vacuum, Crystengcomm 16 (2014) 5466–5474, https://doi.org/10.1039/c4ce00358f.

[56] M. Naguib, O. Mashtalir, M.R. Lukatskaya, B. Dyatkin, C. Zhang, V. Presser, Y. Gogotsi, M.W. Barsoum, One-step synthesis of nanocrystalline transition metal oxides on thin sheets of disordered graphitic carbon by oxidation of MXenes, Chem. Commun. 50 (2014) 7420–7423, https://doi.org/10.1039/c4cc01646g.

[57] J. Sunil, C. Narayana, G. Kumari, K. Jayaramulu, Raman spectroscopy, an ideal tool for studying the physical properties and applications of metal–organic frameworks (MOFs), Chem. Soc. Rev. 52 (2023) 3397–3437, https://doi.org/10.1039/d2cs01004f.

[58] Y. Wang, W. Cao, L. Wang, Q. Zhuang, Y. Ni, Electrochemical determination of 2,4,6-trinitrophenol using a hybrid film composed of a copper-based metal organic framework and electroreduced graphene oxide, Microchim. Acta 185 (2018) 1–9, https://doi.org/10.1007/s00604-018-2857-8.
[59] T. Shen, T. Liu, H. Mo, Z. Yuan, F. Cui, Y. Jin, X. Chen, Cu-based metal–organic framework HKUST-1 as effective catalyst for highly sensitive determination of ascorbic acid, RSC Adv. 10 (2020) 22881–22890, https://doi.org/10.1039/d0ra01260b.
[60] M. Lu, C. Cao, F. Wang, G. Liu, A polyethyleneimine reduced graphene oxide/gold nanocubes based electrochemical aptasensor for chloramphenicol detection using single-stranded DNA-binding protein, Mater. Des. 199 (2021) 109409–109417, https://doi.org/10.1016/j.matdes.2020.109409.
[61] K. Ngamchuea, S. Wannapaiboon, P. Nongkhunsan, P. Hirunsit, I. Fongkaew, Structural and electrochemical analysis of copper-creatinine complexes: application in creatinine detection, J. Electrochem. Soc. 169 (2022) 020567–020577, https://doi.org/10.1149/1945-7111/ac5346.
[62] J. Cruz-Navarro, F. Hernández-García, A. Sánchez-Mora, M. Moreno-Narváez, V. Reyes-Márquez, R. Colorado-Peralta, D. Morales-Morales, Copper-based metal–organic frameworks applied as electrocatalysts for the electroreduction of carbon dioxide (CO2ER) to methane: a review, Methane 3 (2024) 466–484, https://doi.org/10.3390/methane3030027.

Supporting Information

High-performance Nonenzymatic creatinine detection by Cu-MOF@MXene electrochemical sensor

Xianglong Bian[1,#], Dong Yang[2,#], Lin Chen[1], Yingfei Zeng[1], Li Zhu[1], Hua Pei[1], Qianfeng Xia[1], Paul K Chu[3,*], Tingwei Hu[1,4,*]

[1] *NHC Key Laboratory of Tropical Disease Control, School of Tropical Medicine, Hainan Medical University, Haikou 571199, Hainan, China.*

[2] *School of Biomedical Information and Engineering, Hainan Medical University, Haikou 571199, Hainan, China.*

[3] *Department of Physics, Department of Materials Science and Engineering, and Department of Biomedical Engineering, City University of Hong Kong, Tat Chee Avenue, Kowloon, Hong Kong, China*

[4] *State Key Laboratory for Mechanical Behavior of Materials, Xi'an Jiaotong University, Xi'an 710049, Shaanxi, China.*

# Xianglong Bian and Dong Yang contributed equally to this work and should be considered as co-first authors.

* Address correspondence to: htingwei1236@mail.xjtu.edu.cn (Tingwei Hu) and paul.chu@cityu.edu.hk (Paul K Chu)

Fig. S1

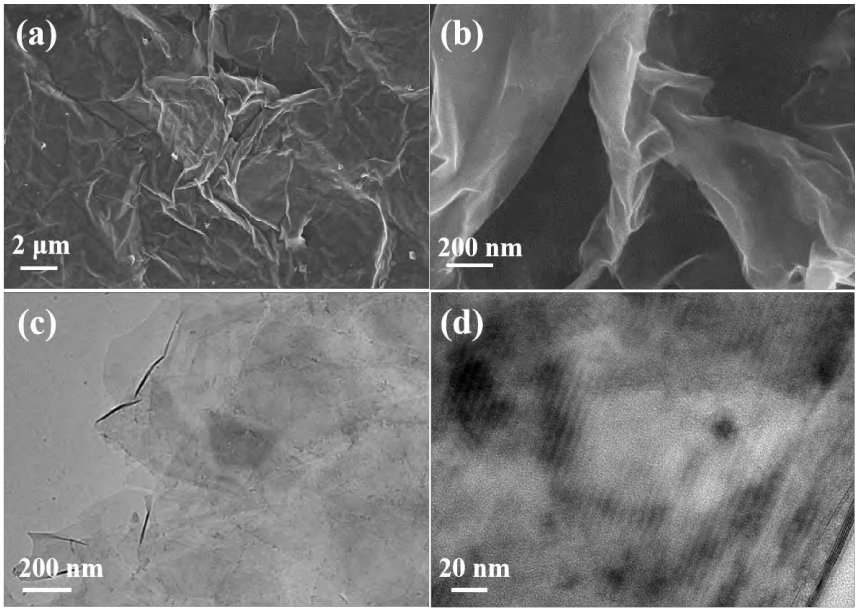

Fig. S1. (a, b) SEM images of MXene; (c, d) TEM images of MXene.

Fig. S2

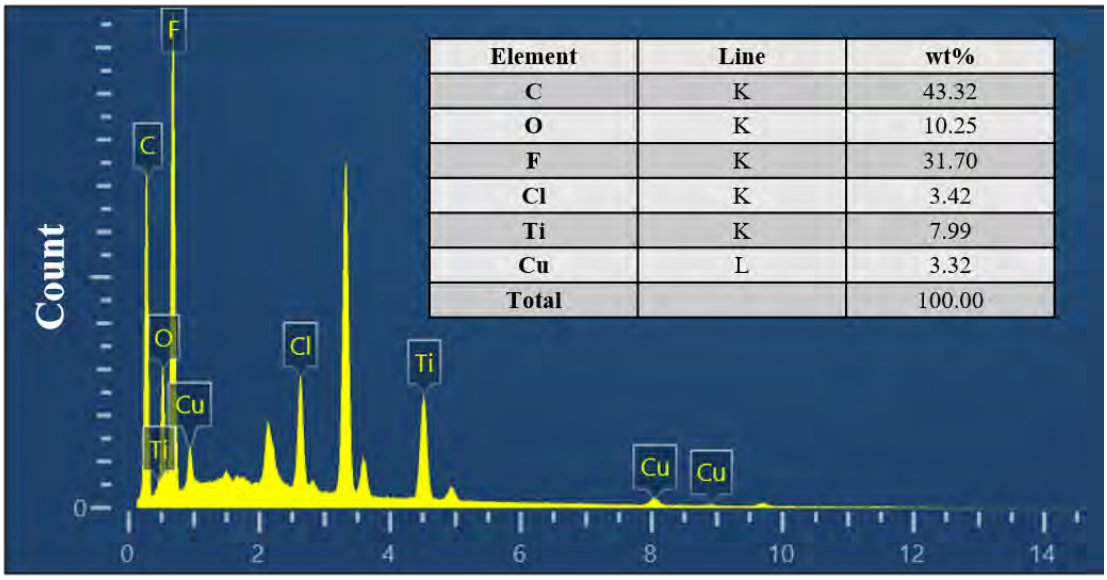

Element	Line	wt%
C	K	43.32
O	K	10.25
F	K	31.70
Cl	K	3.42
Ti	K	7.99
Cu	L	3.32
Total		100.00

Fig. S2. EDS maps of the six elements (C, O, F, Cl, Ti, Cu).

Fig. S3

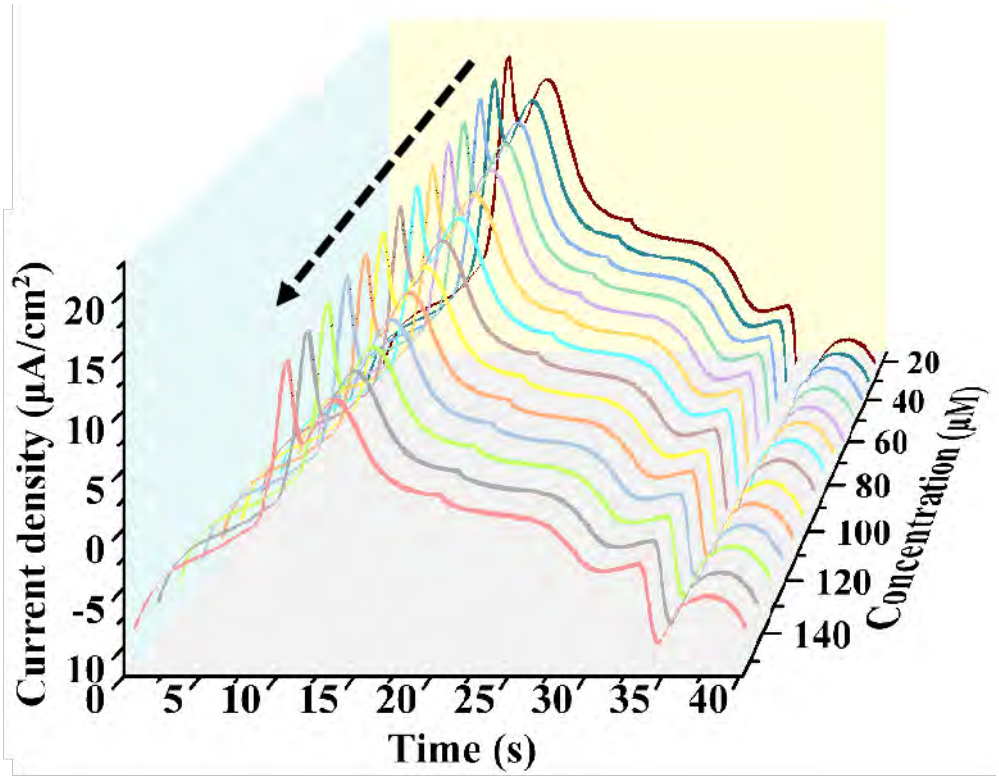

Fig. S3. 3D waterfall plot showing the relationship between current density, creatinine concentration, and time.

Fig. S4

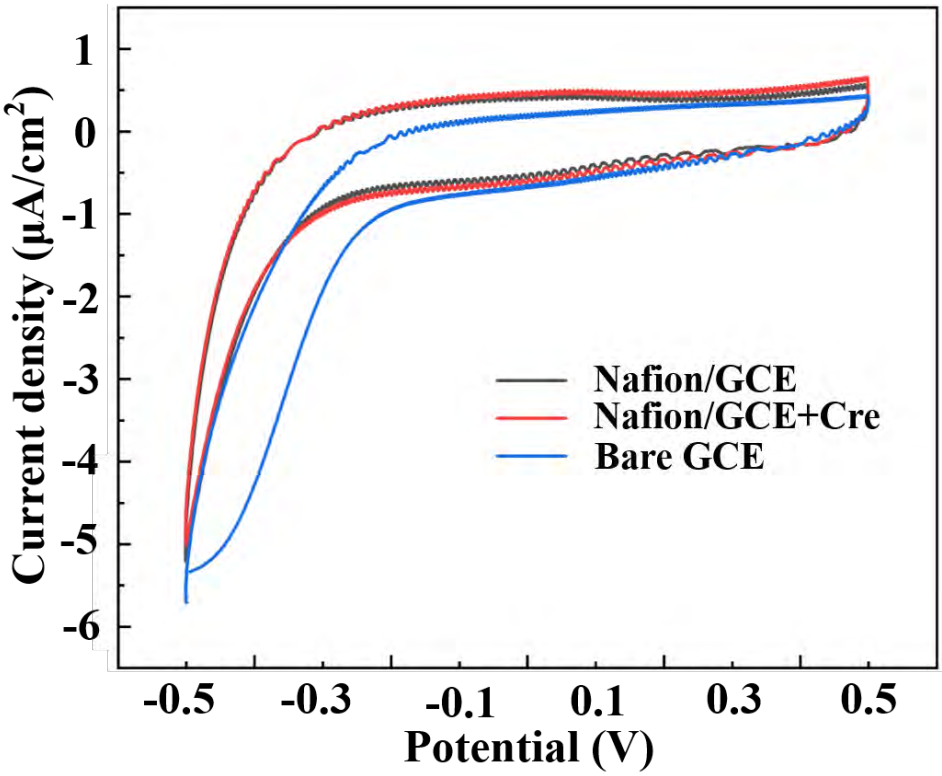

Fig. S4. Comparison of electrochemical performance of glassy carbon electrodes with or without Nafion.

Fig. S5

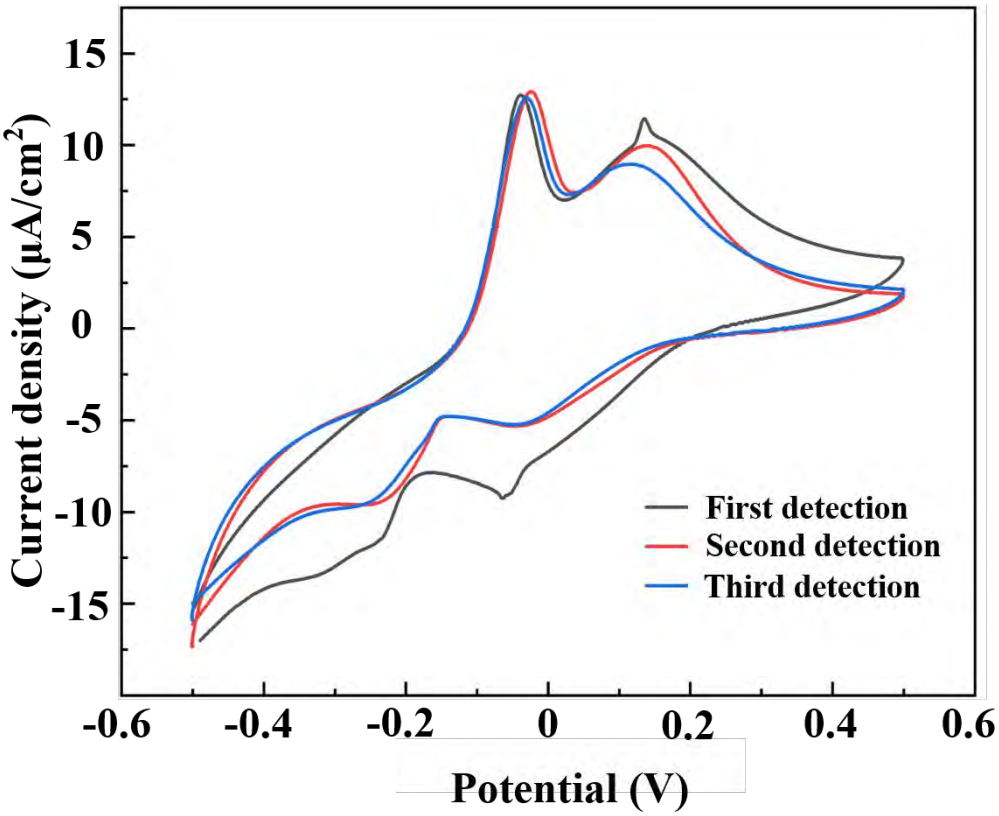

Fig. S5. Long-term stability performance of Cu-MOF@MXene sensor.